Philosophical Magazine
Publication details, including instructions for authors and subscription information:
http://www.tandfonline.com/loi/tphm20

Generalized stacking-faults and screw-dislocation core-structure in bcc iron: A comparison between ab initio calculations and empirical potentials

Lisa Ventelon [a] & F. Willaime [a]
[a] CEA, DEN, Service de Recherches de Métallurgie Physique, F-91191 Gif-sur-Yvette, France
Version of record first published: 30 Mar 2010.

To cite this article: Lisa Ventelon & F. Willaime (2010): Generalized stacking-faults and screw-dislocation core-structure in bcc iron: A comparison between ab initio calculations and empirical potentials, Philosophical Magazine, 90:7-8, 1063-1074

To link to this article: http://dx.doi.org/10.1080/14786431003668793

Philosophical Magazine
Vol. 90, Nos. 7–8, 7–14 March 2010, 1063–1074

Generalized stacking-faults and screw-dislocation core-structure in bcc iron: A comparison between *ab initio* calculations and empirical potentials

Lisa Ventelon* and F. Willaime

CEA, DEN, Service de Recherches de Métallurgie Physique, F-91191 Gif-sur-Yvette, France

(*Received 3 May 2009; final version received 30 September 2009*)

Generalized stacking fault energies and $\frac{1}{2}\langle 111\rangle$ screw dislocation core structures are reported for two sets of models for iron: density functional theory (DFT) calculations and empirical potentials. A thorough comparison between various DFT approaches has been performed on {110} and {211} γ-lines, which give a first indication on dislocation properties: (i) the effect of the exchange-correlation functional, LDA versus GGA, is significant in the pseudopotential approximation but not in the PAW approximation or in paramagnetic calculations; and (ii) the discrepancy due to the basis set between SIESTA and plane-wave results is rather small. Three empirical potentials for iron have been benchmarked on these DFT results. They all yield similar energies, but different shapes for the γ-lines. Using the criterion suggested by Duesbery and Vitek, the γ-line results point to non-degenerate core structures for the DFT calculations and for the Ackland and Ackland–Mendelev potentials but not for the Dudarev–Derlet potential. The direct calculations of the dislocation core structures show that the Ackland potential is an exception to the Duesbery–Vitek rule. More insight into the stability of the core structure can be gained by looking at the response to the polarization of the core. The Dudarev–Derlet and Ackland potentials have similar polarizations, but the energy difference between degenerate and non-degenerate cores is much larger with the Dudarev–Derlet potential, as expected from the γ-lines. The polarizability of the non-degenerate core is smaller with the Ackland–Mendelev potential than in DFT, indicating that the energy landscape is flatter in this direction.

Keywords: generalized stacking fault; γ-surface; bcc iron; dislocation; density functional theory

1. Introduction

The origin of the specific plastic behavior exhibited by body-centred cubic (bcc) metals, and in particular their large Peierls stresses and non-Schmid characteristics, is attributed to core structure effects (see [1–3] for reviews). Atomistic simulations of $\frac{1}{2}\langle 111\rangle$ screw dislocations in bcc metals showed no splitting into well defined partials and stacking faults, but they revealed two types of core configurations with a

*Corresponding author. Email: lisa.ventelon@cea.fr

ISSN 1478–6435 print/ISSN 1478–6443 online

DOI: 10.1080/14786431003668793
http://www.informaworld.com

symmetry consistent with the three-fold ⟨111⟩ axis of the [111] direction. These two types of core are commonly distinguished by the symmetry of their spreading into three {110} planes of the ⟨111⟩ zone. In the first case, the spreading is not centered on the dislocation core. Since this *asymmetric* core exists in two different energetically equivalent symmetry-related variants (Figures 1b and c), it is called *degenerate*. In the second case, the spreading is evenly distributed about a central point, and the core is called *symmetric* or *non-degenerate* (Figure 1a).

Pointing out that the degenerate and non-degenerate cores can be regarded as generalized splittings into, respectively, three fractional dislocations with screw components $\frac{1}{6}\langle 111\rangle$ and six fractional dislocations with screw components $\frac{1}{12}\langle 111\rangle$, Duesbery and Vitek proposed that the preference for one or the other type of core can be related to the γ-surface for the {110} planes into which the core spreads [4]. These authors established the following simple criterion: the degenerate core will be favored if $3\gamma(\mathbf{b}/3) < 6\gamma(\mathbf{b}/6)$ and vice versa for the non-degenerate core. The stacking

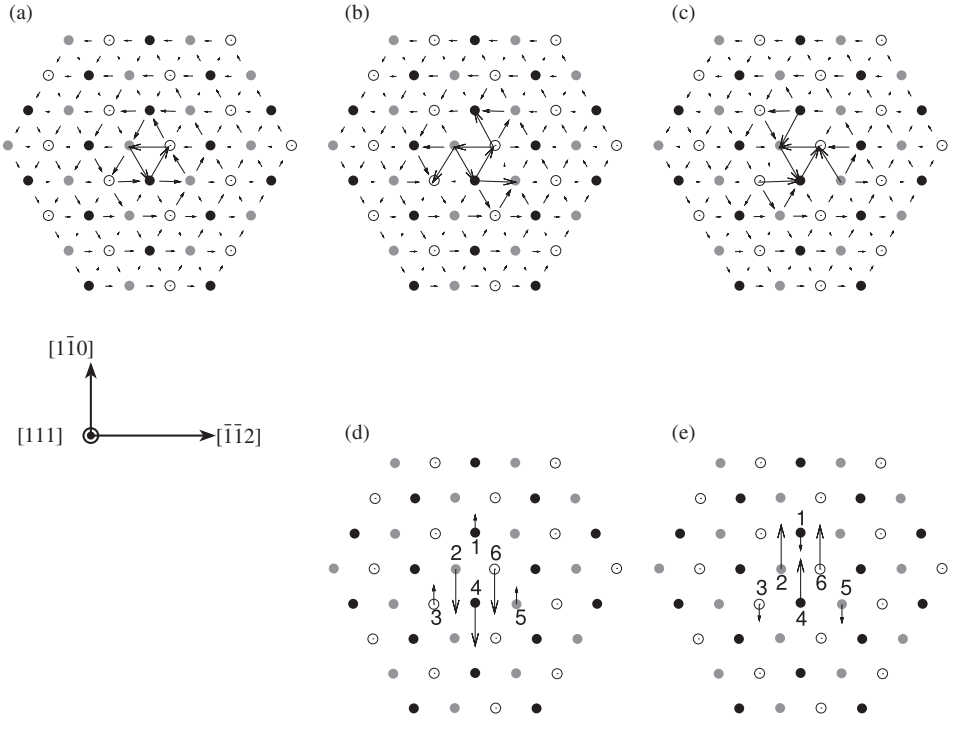

Figure 1. Differential displacement maps for (a) the non-degenerate core structure, and (b) and (c) the two variants of the degenerate core structure obtained using the Dudarev–Derlet potential [20]. (d) and (e) Relaxation maps with respect to anisotropic elasticity positions of the degenerate core structure represented in (b) and (c); the relaxation amplitudes in the [111] direction of the three central [111] atomic columns (labeled 2, 4 and 6) and of the next three columns (labeled 1, 3 and 5) are, respectively, ± 0.251 Å and ∓ 0.099 Å. Displacements smaller than 0.05 Å are omitted in (d) and (e). For comparison, atoms (2, 4 and 6) and (1, 3 and 5) are displaced by, respectively, ± 0.247 Å and ∓ 0.104 Å in the [111] direction using the Ackland potential [17].

fault energies of a bcc lattice being very high, the width of the extended dislocation is at most equal to a few Burgers vectors and there is no sense in speaking of the splitting of a dislocation and of a stacking fault [5,6]. The concept of splitting and the Duesbery–Vitek criterion are therefore more intended to give a qualitative appropriate description of the dislocation properties. However, in practice this criterion was shown, at least initially, to be satisfied in a number of simulations using Finnis–Sinclair or bond order potentials [4,7].

Alternatively, one can compare these two cores to the elasticity solution. Whereas the non-degenerate core essentially corresponds to linear anisotropic elasticity solution, the degenerate core is obtained by an upward or downward displacement along the Burgers vector direction of the three central atomic rows and a downward or upward displacement of the next three atomic rows (Figures 1d and e) [8,9]. Thus, the two types of dislocation core can be distinguished by the *polarization* of the core [8,10]. The polarization, p, is calculated here from the relative displacements in the [111] direction of these two sets of three atomic rows (labeled $\{2,4,6\}$ and $\{1,3,5\}$ in Figures 1d and e) as

$$p = \frac{(d_{12} - d_{23}) + (d_{34} - d_{45}) + (d_{56} - d_{61})}{b}, \tag{1}$$

where $d_{\alpha\beta}$ ($\alpha, \beta = 1, 2, 3, 4, 5$ or 6) is the relative displacement between two neighboring atoms in rows α and β, and b is the amplitude of the Burgers vector. The polarization is assigned to be positive when the relaxation displacement of the three nearest neighbor rows of the dislocation core is parallel to b, and negative when it is antiparallel to b. Since the dislocation energy is independent of the sign of p, dislocations of opposite polarizations are expected to occur at the same frequency. The polarization allows a continuous description from non-degenerate, or *unpolarized*, core ($p = 0$) to fully polarized degenerate core ($|p| = 1$). The core is non-degenerate if the above perturbation mode is stable; this corresponds to a positive curvature in an energy-polarization curve. Moreover the Peierls stress was shown to correlate with the value of the curvature or *polarizability* of the core [10]. Most central-force empirical potentials yield a degenerate core, whereas all the density functional theory (DFT) calculations performed so far (in Fe, Mo, Ta) predict a non-degenerate core [11–15]. But more criteria than simply reproducing the correct core structure are needed to validate empirical potentials used to predict dislocation properties. For instance it was shown that the Mendelev potential for iron, which predicts a non-degenerate core, shows strong discrepancies with DFT calculations concerning the Peierls barrier [16].

The goal of the present paper is to investigate, in the case of iron, how the details of the interatomic bonding influence the properties related to screw dislocations. The long range displacement field of dislocations is related to the elastic constants, and – according to Duesbery and Vitek – the core field is related to generalized stacking faults, or γ-surfaces. These two sets of quantities, which are easy to calculate, can therefore be used as a first indication of the influence that the energetic model used for a given material, iron in the present case, may have on the predicted dislocation structure. In this work, we have thus tested the effects, for DFT based calculations, of the pseudopotential, exchange-correlation functional and basis set. Three empirical interatomic potentials proposed for iron have been selected to be

benchmarked on the present *ab initio* results, namely the extensively used embedded atom method (EAM) potential developed by Ackland et al. [17], the extended version [18] of the recently published improved empirical potential by Ackland, Mendelev et al. [19], and the magnetic potential newly proposed by Dudarev and Derlet [20]. Direct calculations of the core structures are then performed with these three potentials and for DFT calculations only with the SIESTA code, i.e. using the pseudopotential approximation and localized basis sets [21]. Finally, the stability of the core with respect to core polarization is investigated. This allows discrimination between models with similar core structures.

2. Methodology

The present *ab initio* calculations in α-Fe were performed in the DFT framework. They are spin-polarized (unless otherwise noticed), the Hermite–Gaussian smearing technique with a 0.3 eV width was used for electronic density of state broadening, and eight valence electrons were considered for Fe. We have tested the validity of the pseudopotential approximation and basis set used in previous point defect and dislocation SIESTA calculations in iron [16,22,23] by performing a comparison with a plane-wave code (PWSCF [24]) using two levels of approximation: the ultrasoft pseudopotential (US) and projected augmented wave (PAW) method. The SIESTA pseudopotential and basis set are the same as in [22] and [16]; the charge density is represented on a regular real space grid with a grid spacing of 0.06 Å, reduced to 0.03 Å after self-consistency. The PWSCF calculations have been performed with a wavefunction cut-off of 40 Ry. We have also compared the local density approximation (LDA) and the PBE generalized gradient approximation (GGA) schemes to investigate the effect of the exchange-correlation functional. For a given functional, the accuracy is in principle increased when going from SIESTA to PWSCF (more accurate basis set) and from pseudopotentials to all-electron PAW, which performs better in particular for magnetic materials. However, the computational resources required for PWSCF-PAW calculations being at least one order of magnitude larger than for SIESTA calculations, the dislocation calculations have been performed only with the SIESTA code in the present study.

The DFT elastic constants are obtained from a fourth order polynomial fit performed over the energies calculated for nine values of the strain ranging from -2% to $+2\%$ and a $16 \times 16 \times 16$ k-point grid.

For the γ-surface calculations, as well as for the dislocation calculations, the same cells are used for the empirical potentials and DFT approaches. The γ-surfaces depict the variation of the energy obtained when two parts of a crystal, separated by a virtual cut plane, are rigidly displaced with respect to each other. The cell geometries used for the calculations of the $\{110\}$ and $\{211\}$ γ-surfaces are represented in Figure 2. Periodic boundary conditions are used along the cut plane, and a slab geometry is used with free surfaces. For each displacement vector, $\boldsymbol{f}$, only relaxations perpendicular to the cut plane are allowed. The stacking sequences are, respectively, of ABA and ABCDEFA types. The results are presented for 10 and 12 atomic layer slabs, respectively. The comparison with 18 atomic layer supercell results shows that the calculation is well converged with respect to supercell size. The

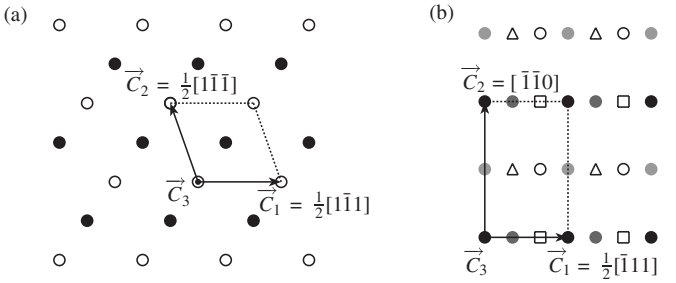

Figure 2. Projection normal to the (a) (110) and (b) ($\bar{1}1\bar{2}$) plane of the supercells used for γ-surface calculations. The cell vectors used for the (110) and ($\bar{1}1\bar{2}$) γ-surface calculations are designated by ($\vec{C}_1$, $\vec{C}_2$, $\vec{C}_3$).

Table 1. Comparison between experiments and various DFT calculations of bulk properties in α-Fe: lattice constant, a_o (Å), bulk modulus, B (GPa), magnetic moment, μ (μ_B), elastic constants, C_{11}, C_{12}, C', C_{44} (GPa), ⟨111⟩ shear modulus, G (GPa), and anisotropy ratio, A.

Method	a_o	B	μ	C'	C_{44}	G	A
SIESTA GGA	2.88	185	2.32	53	76	60	1.43
SIESTA LDA	2.80	245	2.08	68	112	83	1.64
PWSCF US-GGA	2.85	177	2.26	55	70	60	1.27
PWSCF US-LDA	2.77	254	2.10	71	93	79	1.31
PWSCF PAW-GGA	2.84	198	2.17	70	83	74	1.19
PWSCF PAW-LDA	2.76	248	2.00	71	102	81	1.44
Experiment	2.87	168	2.22	49	116	71	2.37

DFT {110} and {211} γ-surface calculations have been carried out using $12 \times 12 \times 1$ and $12 \times 8 \times 1$ shifted k-point grids, respectively.

For the dislocation calculations, we used periodic cells containing 273 atoms per unit length with a quadrupolar arrangement of dislocations [16,23]. In the DFT calculations, the length of the cell vector is b along the dislocation line and a $2 \times 2 \times 16$ k-point grid is used.

3. Results and discussion

3.1. *Bulk properties*

The Fe bulk properties obtained for the various types of DFT approaches used in the present study are reported in Table 1. In agreement with previous studies, we find a tendency for LDA to underestimate the lattice parameter and to overestimate the bulk modulus with respect to experiments, these two quantities being much better reproduced within GGA. As a consequence, the magnetic moment is always smaller within LDA than GGA, both being close to the experimental value. The agreement with experiments obtained with SIESTA on the elastic constants is good, but one of the points we wanted to investigate is whether it could be improved in particular

on C_{44}: the data are somehow scattered with no major advantage of either of the approaches, which may indicate that it is necessary to include semi-core states in the valence band to get closer to experiments. One of the consequences is that the rather large experimental value of the anisotropy ratio, $A = C'/C_{44}$, is never really well reproduced. However the displacement field of screw dislocation is related to the shear modulus in the $\langle 111 \rangle$ direction, $G = (C_{11} - C_{12} + C_{44})/3$, which is quite well reproduced in all approaches.

3.2. *DFT γ-surfaces*

The DFT results of the $\langle 111 \rangle$ cross-sections of the $\{110\}$ and $\{211\}$ γ-surfaces are shown in Figure 3. All DFT approaches yield very similar shapes, which agree with previous calculations [13,25]; they mostly differ by their amplitude. No intermediate minima are found in both $\{110\}$ and $\{211\}$ γ-lines, and maximum energies are obtained at $f/b = 0.5$ in the $\{110\}$ γ-lines. The maximum energies are shifted to the left in the $\{211\}$ γ-lines, a consequence of the twinning-antitwinning slip asymmetry. As a result of the absence of a minimum, no metastable stacking fault on the $\{110\}$ and $\{211\}$ planes, and so no dissociation into partial dislocations, are expected, as it is generally accepted in bcc materials [2]. In the pseudopotential approximation, the effect of the exchange-correlation functional is significant: the stacking fault energies are reduced by up to 25% from LDA to GGA with SIESTA. The discrepancy between SIESTA and PWSCF-US results is rather small in comparison and these results agree quantitatively with the results obtained by Frederiksen and Jacobsen [13]. On the other hand, the LDA and GGA results are very similar in the PAW approach and they lie in between the LDA and GGA pseudopotential results. The relaxation amplitude is similar between SIESTA and PWSCF, as shown in Table 2 for the GGA $\{110\}$ and $\{211\}$ γ-lines.

The complete γ-surfaces obtained using the SIESTA code are represented in Figure 4. Both $\{110\}$ and $\{211\}$ γ-surfaces are remarkably similar in their shape for

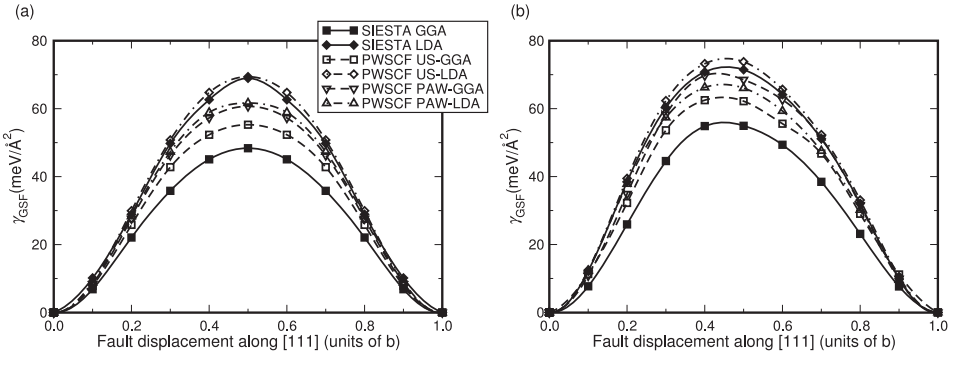

Figure 3. Relaxed (a) $\{110\}$ and (b) $\{211\}$ γ-lines along the [111] direction obtained from DFT calculations for Fe using, respectively, SIESTA, PWSCF-US and PWSCF-PAW, and two exchange-correlation functionals (LDA versus GGA). The $\boldsymbol{x}$ axis is given in units of the Burgers vector 1/2[111].

LDA and GGA, as well as for other DFT approaches and empirical potentials (not shown) [16]. The {110} γ-surfaces are centrosymmetric, so that the surfaces are invariant with the direction of slip. The almost circular contours of constant γ_{GSF} indicate the independence of γ with the direction of the fault vector $\boldsymbol{f}$. The {211} γ-surfaces are asymmetric, related to the twinning-antitwinning asymmetry, as shown previously in the ⟨111⟩ cross-sections.

Table 2. Relaxation amplitude[a] calculated from the {110} and {211} γ-lines along the [111] direction using SIESTA and PWSCF within GGA.

		PWSCF	
	SIESTA	US	PAW
{110}	14.9	10.5	15.0
{211}	15.8	12.0	18.5

Notes: [a]The relaxation amplitude is defined in meV Å^{-2} as: $\gamma^{ur}_{GSF}(b/2) - \gamma^{r}_{GSF}(b/2)$, where *ur* and *r* denote the unrelaxed and relaxed γ-lines, respectively.

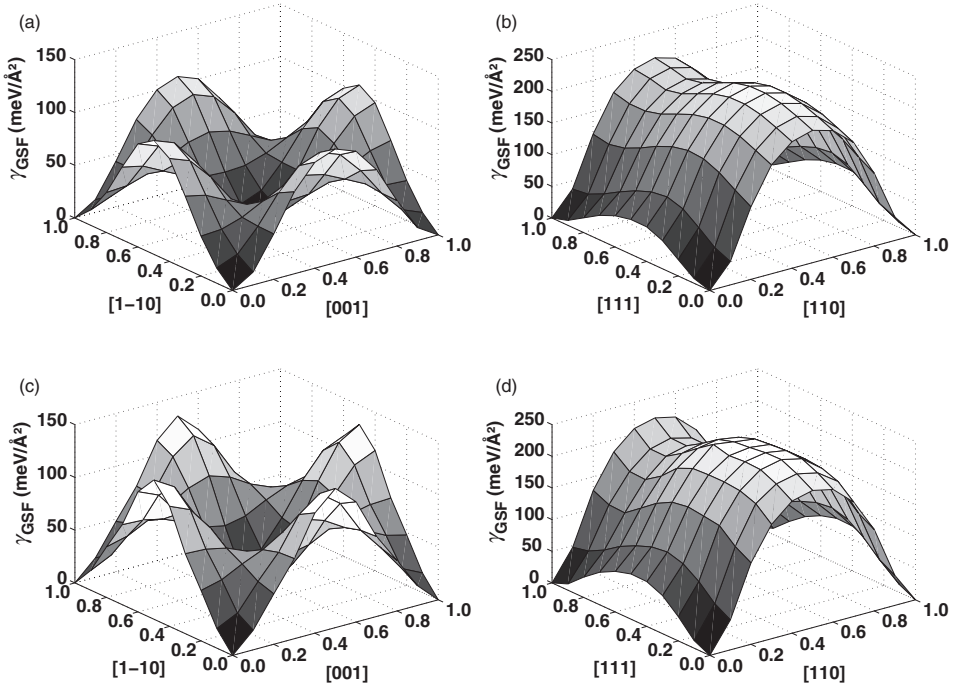

Figure 4. Relaxed {110} (left) and {211} (right) γ-surfaces using (a) and (b) SIESTA DFT-GGA, and (c) and (d) SIESTA DFT-LDA framework. The $\boldsymbol{x}$ and $\boldsymbol{y}$ axes are given in reduced units.

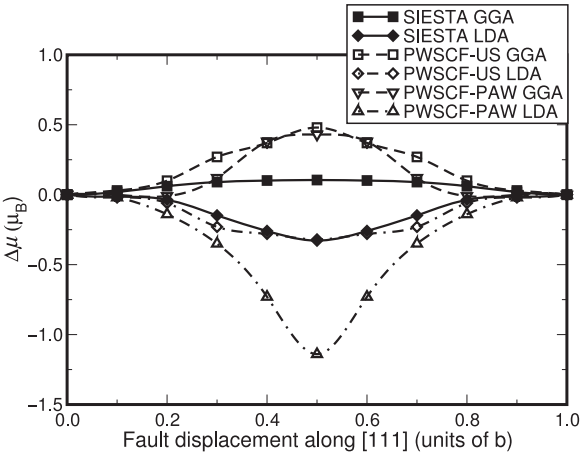

Figure 5. Change in total magnetic moment in a 10-atom unit cell, due to stacking fault in the {110} plane. The ***x*** axis is given in units of the Burgers vector 1/2[111].

We have also investigated the effect of magnetism, concentrating on the {110} γ-line. From unrelaxed paramagnetic PWSCF calculations (not shown) it can be seen that: (i) for a given exchange-correlation functional the US and PAW results are identical within less than $\approx 1\,\mathrm{meV/\AA^2}$; and that (ii) the two functionals differ by at most $5\,\mathrm{meV/\AA^2}$ as in the PAW case for ferromagnetic calculations. This suggests that the significant effect of the exchange-correlation functional observed in the pseudopotential ferromagnetic calculations as well as the discrepancy between PAW and pseudopotential results in ferromagnetic calculations, originate from magnetic interactions. Analyzing the average magnetic moment in the ferromagnetic calculations, we found that the average value is reduced with respect to the bulk in the LDA approximation, and it is enhanced in the GGA approximation (see Figure 5). In the LDA case, the reduction is more than three times larger for the PAW than for the pseudopotential calculations. Further investigations are required to understand the origin and consequences of these complex magnetic behaviors. However, assuming that the most accurate description of the γ-lines is given by the PAW calculations, it can be concluded that LDA and GGA pseudopotential calculations are both equally good approximations, which are bracketing the PAW results. For these reasons, DFT results for dislocation calculations are expected to be well bracketed by LDA and GGA SIESTA results.

3.3. *γ-surfaces: comparison with empirical potentials*

The empirical potential results for the {110} and {211} γ-lines along the [111] direction are compared with the PAW-GGA calculations in Figure 6. The scatter in amplitude is similar to that among DFT results. All empirical potential results are slightly lower than the PAW-GGA value. The shape of the Ackland γ-lines looks very similar to the DFT ones, whereas the Ackland–Mendelev lines are rather flat at their maximum and the Dudarev–Derlet are convex around b/3 and 2b/3. In order to

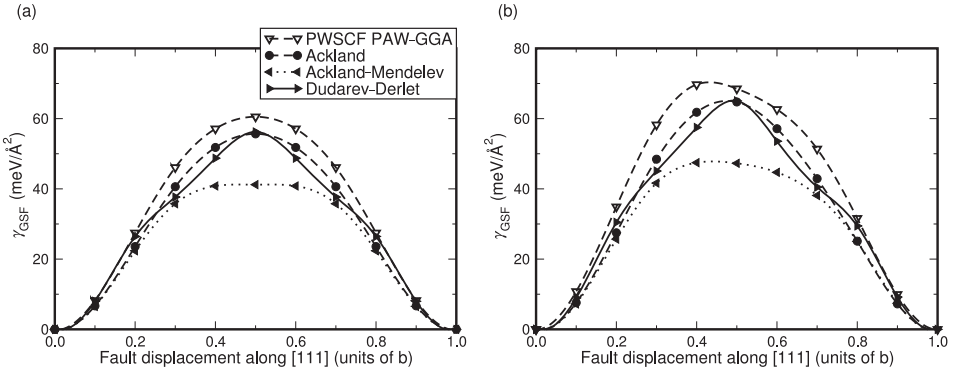

Figure 6. Relaxed (a) {110} and (b) {211} γ-lines along the [111] direction using PAW-GGA, and the Ackland potential, the Ackland–Mendelev potential, and the Dudarev–Derlet potential.

Table 3. Shape and asymmetry factors of the {110} and {211} γ-lines (see, respectively, Equations (3) and (2) for definitions) calculated from the relaxed {110} and {211} γ-lines along the [111] direction and relationship to the degeneracy of the dislocation core structure.

	SIESTA		PWSCF US		PWSCF PAW		Empirical potential		
	GGA	LDA	GGA	LDA	GGA	LDA	Ackland	Ackland–Mendelev	Dudarev–Derlet
$(\Delta\gamma/\gamma)^{\{110\}}$(%)	16.4	21.2	16.9	20.2	18.1	17.8	25.0	11.9	−0.7
$(\Delta\gamma/\gamma)^{\{211\}}$(%)	13.7	14.0	13.2	15.5	11.7	16.7	10.9	8.0	9.3
Degenerate	no	no	/	/	/	/	yes	no	yes

quantify the asymmetry of the {211} γ-lines, the following asymmetry factor is commonly used [13]:

$$\frac{\Delta\gamma^{\{211\}}}{\gamma^{\{211\}}} = 2\frac{\gamma(b/3) - \gamma(2b/3)}{\gamma(b/3) + \gamma(2b/3)}. \tag{2}$$

The asymmetry of the {211} γ-surfaces along the [111] direction – known as the twinning-antitwinning asymmetry – indicates that shearing in the positive [111] direction is not equivalent to shearing in the opposite direction (except in the {110} planes). This asymmetry is found to be larger in DFT calculations than using empirical potentials, as shown in Table 3: it amounts to about 13.7% for SIESTA-GGA, but only about 8.0% using the Ackland–Mendelev potential. Since this asymmetry constitutes the primary reason for the breakdown of the Schmid law, the deviation from Schmid law is expected to be weaker with empirical potential than with DFT.

3.4. *Symmetry and stability of dislocation cores*

By analogy with the asymmetry factor, we can define a shape factor for the {110} γ-lines, which characterizes the tendency of having a non-degenerate core according to the Duesbery–Vitek criterion:

$$\frac{\Delta\gamma^{\{110\}}}{\gamma^{\{110\}}} = \frac{\gamma(b/3) - 2\gamma(b/6)}{\gamma(b/3)}, \tag{3}$$

a negative value meaning a tendency for a degenerate core. As seen in Table 3, it is only negative in the case of the Dudarev–Derlet potential, as a result of the characteristic 'shoulder' observed around b/6 in Figure 6a. As expected from the Duesbery–Vitek criterion, the Dudarev–Derlet core structure is found to be degenerate (see the relaxation map in Figure 1d). The Duesbery–Vitek criterion is also valid for the Ackland–Mendelev potential, SIESTA-GGA and SIESTA-LDA since in these three cases $3\gamma(\mathbf{b}/3) > 6\gamma(\mathbf{b}/6)$ and the core configuration is non-degenerate [16,26]. On the other hand, the Ackland potential surprisingly does not satisfy the Duesbery–Vitek criterion: the dislocation core structure falls indeed into a degenerate core configuration, similar to that of Dudarev–Derlet potential (see Figure 1d) although $3\gamma(\mathbf{b}/3) > 6\gamma(\mathbf{b}/6)$.

When the core is degenerate, it is interesting to gain more insight into the relative stability between the degenerate (stable) and the non-degenerate (unstable) core configurations. The non-degenerate configuration corresponds to the saddle point configuration for one variant of the degenerate core to flip into the other variant, which is symmetric with respect to the $[10\bar{1}]$ diad. Calculations of the corresponding energy barriers have been performed using the drag method within the cluster approach. The Dudarev–Derlet potential yields an energy difference four times larger than the Ackland potential (Figure 7a). This result is consistent with the

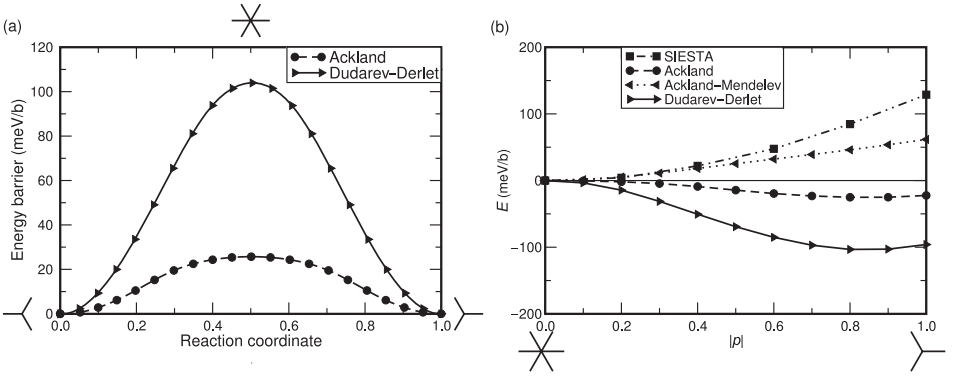

Figure 7. (a) Energy barrier per dislocation between the two variants of the degenerate core structure, calculated with the Ackland and the Dudarev–Derlet potentials. (b) Dependence of the dislocation core energy with the modulus of its polarization calculated using SIESTA and the three empirical potentials. The SIESTA-GGA and SIESTA-LDA results are identical within less that 5 meV/b; they are therefore represented on the same curve. These calculations have been performed using the quadrupolar distribution of dislocation dipoles, with a cell containing 273 atoms/b.

stronger tendency of the Dudarev–Derlet potential for degenerate core predicted by the Duesbery–Vitek criterion.

A similar insight can also be gained when the non-degenerate core is stable. It can be obtained by calculating the dependence of the dislocation core energy with its polarization [10]. An initial displacement along the [111] direction is imposed on atoms 2, 4 and 6 in Figure 1, and an opposite displacement, with half amplitude, is imposed on atoms 1, 3 and 5. Then a constrained minimization is performed such that the polarization p is kept constant while all other degrees of freedom are relaxed. The result obtained for the three empirical potentials, SIESTA-LDA and SIESTA-GGA is represented in Figure 7b. The SIESTA-LDA and SIESTA-GGA results are actually identical, within 5 meV/b. As expected, for the Dudarev–Derlet and Ackland potentials, the energy difference between the two types of cores is the same as in Figure 7a. The position of the minimum – around $|p| = 0.85$ – is the same for both potentials, although one minimum is much deeper than the other. In the Ackland–Mendelev and SIESTA cases, these calculations confirm that the stable core is totally unpolarized and they prove that there is no metastable polarized core. A quantitative discrepancy is observed between these two non-degenerate cores: the energy increase is about twice lower for the Ackland–Mendelev potential than for SIESTA. This indicates that the displacement mode involved in the non-degenerate to degenerate transformation is much softer for the Ackland–Mendelev potential and the question is open to whether it can become unstable when, e.g. the temperature is increased or when an external stress is applied. According to the correlation proposed by Wang et al., a lower Peierls stress is expected for the Ackland–Mendelev potential [10].

4. Conclusion

More insight has be gained into the effect of interatomic interactions on the properties of screw dislocation cores and related properties in bcc Fe. From a thorough comparison between various DFT approaches on {110} and {211} γ-lines, it is concluded that magnetism plays a significant role in the discrepancy observed between LDA and GGA results on the one hand, and between pseudopotential and PAW results on the other. On the basis of this comparison, the SIESTA approach used in previous and present dislocation core calculations seems quite reliable, in particular, if the calculations are repeated using both exchange-correlation functionals.

The link between the value of $3\gamma(\mathbf{b}/3) - 6\gamma(\mathbf{b}/6)$ and the degeneracy of the dislocation core is at most qualitative, and it is shown that the well known Ackland potential is an exception to the Duesbery–Vitek rule relating a positive sign to a non-degenerate core. A hierarchy between interaction models can be established concerning the stability/instability of the non-degenerate core from the dependence of core energy with polarization. The Dudarev–Derlet non-degenerate core is highly unstable and falls into a deep degenerate core miminum with polarization $p = 0.8$. A similar behavior is obtained for the Ackland potential, but the minimum is much less pronounced. The Mendelev–Ackland non-degenerate core can be viewed as equally

stable as the Ackland degenerate core, and the SIESTA-GGA non-degenerate core is much more stable with respect to the displacement toward the degenerate core.

Acknowledgements

We thank C.C. Fu (CEA/Saclay, France) for her help with the SIESTA code and L. Paulatto (SISSA and DEMOCRITOS, Trieste, Italy) for providing PAW datasets for Fe. This work was funded by the EFDA MAT-REMEV programme and by the SIMDIM project under contract No. ANR-06-BLAN-250. It was performed using HPC resources from GENCI-CINES (Grant 2009-096020).

References

[1] V. Vitek, Cryst. Latt. Def. 5 (1974) p.1.
[2] J.W. Christian, J. Metall. Trans. A 14 (1983) p.1237.
[3] M.S. Duesbery, *The dislocation core and plasticity*, in *Dislocations in Solids*, Vol. 8, F.R.N. Nabarro, ed., Elsevier, Amsterdam, 1989, p.67.
[4] M.S. Duesbery and V. Vitek, Acta Mater. 46 (1998) p.1481.
[5] F. Kroupa and V. Vitek, Czech. J. Phys. 14 (1964) p.337.
[6] V. Vitek and F. Kroupa, Czech. J. Phys. 18 (1968) p.464.
[7] V. Vitek, Phil. Mag. 84 (2004) p.415.
[8] A. Seeger and C. Wüthrich, Nuovo Cim. 33B (1976) p.38.
[9] S. Takeuchi, Phil. Mag. A 39 (1979) p.661.
[10] G. Wang, A. Strachan, T. Cagin and W.A. Goddard III, Phys. Rev. B 67 (2003) p.140101.
[11] S. Ismail-Beigi and T.A. Arias, Phys. Rev. Lett. 84 (2000) p.1499.
[12] C. Woodward and S.I. Rao, Phys. Rev. Lett. 88 (2002) 216402.
[13] S.L. Frederiksen and K.W. Jacobsen, Phil. Mag. 83 (2003) p.365.
[14] D.E. Segall, A. Strachan, W.A. Goddard III, S. Ismail-Beigi and T.A. Arias, Phys. Rev. B 68 (2003) 014104.
[15] C. Domain and G. Monnet, Phys. Rev. Lett. 95 (2005) 215506.
[16] L. Ventelon and F. Willaime, J. Comput. Aided Mater. Des. 14 (2007) p.85.
[17] G.J. Ackland, D.J. Bacon, A.F. Calder and T. Harry, Phil. Mag. A 75 (1997) p.713.
[18] G.J. Ackland, M.I. Mendelev, D.J. Srolovitz, S. Han and A.V. Barashev, J. Phys. Condens. Matter 16 (2004) p.S2629.
[19] M.I. Mendelev, S. Han, D.J. Srolovitz, G.J. Ackland, D.Y. Sun and M. Asta, Phil. Mag. 83 (2003) p.3977.
[20] S.L. Dudarev and P.M. Derlet, J. Phys. Condens. Matter 17 (2005) p.7097.
[21] J.M. Soler, E. Artacho, J.D. Gale, A. Garca, J. Junquera, P. Ordejón and D. Sánchez-Portal, J. Phys. Condens. Matter 14 (2002) p.2745.
[22] C.-C. Fu, F. Willaime and P. Ordejón, Phys. Rev. Lett. 92 (2004) 17553.
[23] E. Clouet, L. Ventelon and F. Willaime, Phys. Rev. Lett. 102 (2009) 055502.
[24] http://www.pwscf.org
[25] J.-A. Yan, C.-Y. Wang and S.-Y. Wang, Phys. Rev. B 70 (2004) p.174105.
[26] J. Chaussidon, M. Fivel and D. Rodney, Acta Mater. 54 (2006) p.3407.